Single Frequency-based Visual Servoing for Microrobotics Applications

Valérian Guelpa[1], Guillaume J. Laurent[1], Brahim Tamadazte[1],
Patrick Sandoz[2], Nadine Le Fort-Piat[1] and Cédric Clévy[1]

Abstract— Recently, high resolution visual methods based on direct-phase measurement of periodic patterns has been proposed with successful applications to microrobotics. This paper proposes a new implementation of direct-phase measurement methods to achieve 3-DoF (degrees of freedom) visual servoing. The proposed algorithm relies on a single frequency tracking rather than a complete 2D discrete Fourier transform that was required in previous works. The method does not require any calibration step and has many advantages such as high subpixelic resolution, high robustness and short computation time. Several experimental validations (in favorable and unfavorable conditions of use) were performed using a XYθ microrobotic platform. The obtained results demonstrate the efficiency of the frequency-based controller, this in term of accuracy (micrometric error), convergence rate (30 iterations in nominal conditions) and robustness.

I. INTRODUCTION

The need for accurate microrobotic cells increases rapidly to perform complex tasks, such as microassembly, characterization of MEMS and MOEMS, biological micromanipulation, etc. However, despite positioning stages having individual high repeatability and accuracy, microrobotic cells made of an assembly of several stages (in serial or in parallel) require dedicated control strategies to achieve high accuracy in all DoF. The control strategies are generally classified into open and closed-loop schemes [1]. The former relies on robot calibration that consists in locating the end-effector of the manipulator in the Cartesian space and then in compensating errors with an identified position-dependent model [2], [3], [4]. Closed-loop approaches require an exteroceptive sensor to servo the end-effector position in real-time. Visual servoing is widely used to that purpose at both macro and microscales.

Visual servoing arises from the integration of different research areas including image processing, computer vision, robotics, sensor integration and control theory [5]. Certainly, the most popular visual servoing schemes concern: 1) image-based visual servoing (IBVS) which uses 2D visual features (points, lines, moments) to build the control law, 2) pose-based visual servoing (PBVS) which requires an additional step i.e., the estimation of the 3D information (pose of the object in the Cartesian space).

More recently, new visual servoing paradigms have been reported in the literature. Instead of using geometric visual features, they use the pure image information e.g., pixel-intensity [6], [7], mutual information [8], etc. These approaches allow to overcome the traditional visual servoing limitations: the choice of the visual information, their extraction and matching over time. These steps can be summarized by the term visual tracking [9]. Also, the use of global image information as visual signal input in the control loop allows increasing the accuracy of the controller thanks to the visual features redundancy. Others original global image visual servoing techniques were treated in the literature demonstrating real scientific and technical added-values. For instance, using the Fourier phase-correlation [10] as well as using wavelet coefficients [11] or shearlet ones [12].

In other scientific fields, high resolution visual methods based on direct-phase measurement of periodic patterns have been proposed by different authors [13], [14], [15], [16]. Applications to position-referenced microscopy [17], microrobot calibration [3] and microforce measurement [18] have been reported demonstrating very high resolutions and accuracies.

In this paper, we propose a recursive implementation of direct-phase measurement method to achieve 3-DoF visual servoing. Thereby, the image position is computed over time by firstly tracking the angle and frequencies of the signal then extracting the position of a pattern from phase shift of its image. The proposed algorithm relies on a single frequency tracking rather than a complete 2D discrete Fourier transform that was required in previous works [17], [3].

The method has many advantages such as high subpixelic resolution, high robustness and short computation time. In addition, contrasting with the state-of-the-art in this field, the proposed visual servoing method does not require any calibration step e.g., camera intrinsic matrix or camera/robot transformation one.

The developed materials are experimentally validated using 3-DoF microrobotic platform. To be able to judge the controller's performances, several validation scenarios are performed in both favorable (small displacements, stable illumination, etc.) and unfavorable (lighting changes, occlusions, etc.) conditions of use. The expected results include accuracy, robustness and a good convergence rate.

In the remainder of this paper, Section II introduces the general basics of the position and frequency tracking in the case of 1-D signals when Section III extends this approach for 2-D signals i.e., an image. Section IV gives the different steps followed to build the visual servoing controller. The developed testbench as well as the experimental validation of the proposed controller are discussed in Section V.

[1] Automation and Micro-Mechatronics Systems Department, FEMTO-ST Institute, Univ. Bourgogne Franche-Comté, UMR CNRS 6174, ENSMM, Besançon, France
[2] Applied Mechanics Department, FEMTO-ST Institute, Univ. Bourgogne Franche-Comté, UMR CNRS 6174, ENSMM, Besançon, France

II. POSITION AND FREQUENCY TRACKING IN 1-D

This section introduces the position and frequency tracking of a one-dimensional periodic signal. This latter is intended to be the image of a periodic pattern.

A. Position Tracking

Let s_n be a 1-D spatial signal (pixel values) of size N, its Discrete Fourier Transform (DFT) for frequency k is given by:

$$S_k = \mathcal{F}(\{s_n\})_k = \sum_{n=0}^{N-1} s_n \ e^{-2\pi i \frac{kn}{N}}, \quad k \in [0, N-1] \quad (1)$$

If the signal s_n is shifted from an initial position, the spatial displacement d produces a linear phase variation in the Fourier domain:

$$\mathcal{F}(\{s_{n-d}\})_k = S_k \ e^{-2\pi i \frac{kd}{N}} \quad (2)$$

In other words, a spatial shift d induces only a phase change equal to $2\pi \frac{kd}{N}$ in the frequency domain.

Thanks to this linear relationship, the spatial shift is encoded into the phase of the Fourier transform. Different approaches were proposed to measure displacements through the phase term. They differ mainly in the number of considered spectral components. Fast approaches consider a single spectral component instead of a complete Fourier transform. In this case, the displacements retrieved are subject to phase ambiguities that limit the actual unambiguous measurement range as described below. However, this limitation is not critical for tracking applications if the motion between two consecutive frames remains sufficiently small (i.e., smaller than half the period).

If the signal is periodic with a frequency k, the phase change can be retrieved from of a single-frequency spectral computation with a very high resolution and signal-to-noise ratio. Given the frequency k of the signal, the phase ϕ can be estimated (estimated values will be written with ˆ) by:

$$\hat{\phi}_0 = \arg \sum_{n=0}^{N-1} s_n \ h_n \ e^{-2\pi i \frac{kn}{N}} \quad (3)$$

where h_n is a Gaussian window (standard deviation σ) given by:

$$h_n = e^{-\left(\frac{n-N/2}{\sigma}\right)^2} \quad (4)$$

This window function enlarges the frequency band of the analysis that makes the phase computation more robust especially when the frequency of the signal is not exactly k.

As the spatial shift is linearly dependent to the phase, we get:

$$\hat{d} = \frac{\lambda \hat{\phi}_0}{2\pi} + p\,\lambda \quad (5)$$

where $\lambda = N/k$ is the period of the signal in pixels and p is an unknown integer since the signal periodicity involves an ambiguity of λ on the knowledge of its position. This fact limits the tracking range to a maximal shift of $\lambda/2$ between two consecutive frames.

B. Frequency Tracking

The phase estimation depends on the frequency estimation. The DFT spectrum is intrinsically discrete in the frequency domain and is limited by its natural resolution $(2\pi/N)$. Thus, the accurate estimation of the frequency of a sinusoid involves interpolation using several samples of the DFT spectrum. Many frequency estimation algorithms have been proposed in the literature. Since we are interested in real-time tracking, a fast one is required. However, since the frequency changes slightly from one frame to another, an iterative method is sufficient.

It has been shown in [19] that the frequency f of a real continuous-spatial signal $s(x)$ is:

$$f = \frac{1}{2\pi} \frac{\mathrm{d}\varphi}{\mathrm{d}x} \quad (6)$$

where φ is the phase of the signal relative to the analysis function.

Good approximations to the differentiation operation in discrete-time can be obtained by using a phase differencing operation [20]. This approach is very computationally efficient and generally yields better noise performance than spatial filters. The forward, backward and central finite differences are commonly used for phase differentiation. The central finite difference (CFD) is defined by:

$$\hat{k} = \frac{1}{4\pi} \left(\hat{\phi}_1 - \hat{\phi}_{-1} \right) \quad (7)$$

with $\hat{\phi}_1$ and $\hat{\phi}_{-1}$ defined by:

$$\hat{\phi}_x = \arg \sum_{n=0}^{N-1} s_{n+x} \ h_n \ e^{-2\pi i \frac{kn}{N}} \quad (8)$$

In this equation adapted from (3), the vectors are zero completed to have the same size and the index x allows computing the phase in different locations of the signal. This scheme is unbiased and must be preferred to forward and backward ones.

III. POSITION AND FREQUENCY TRACKING IN 2-D

This section extends the position and frequency tracking from 1-D periodic signal to 2-D, allowing measurements along two translation axes and one rotation axis.

A. 2-D Position Tracking

Let $s_{n,m}$ be a 2-D spatial signal (still pixel values, size $N \times M$). Its DFT for frequencies k_1 and k_2 is given by:

$$S_{k_1,k_2} = \sum_{n=0}^{N-1} \sum_{m=0}^{M-1} s_{n,m} \cdot e^{-2\pi i \left(\frac{k_1 n}{N} + \frac{k_2 m}{M} \right)} \quad (9)$$

Similarly to the 1-D tracking, spatial shifts along a first axis of the pattern have a linear impact on the phase of the image (see Fig. 1), that is obtained by:

$$\hat{\phi}_{x,y,\theta} = \arg \sum_{n=0}^{N-1} \sum_{m=0}^{M-1} s_{n+x,m+y} \cdot h_{n,m} \cdot a_{n,m,\theta} \quad (10)$$
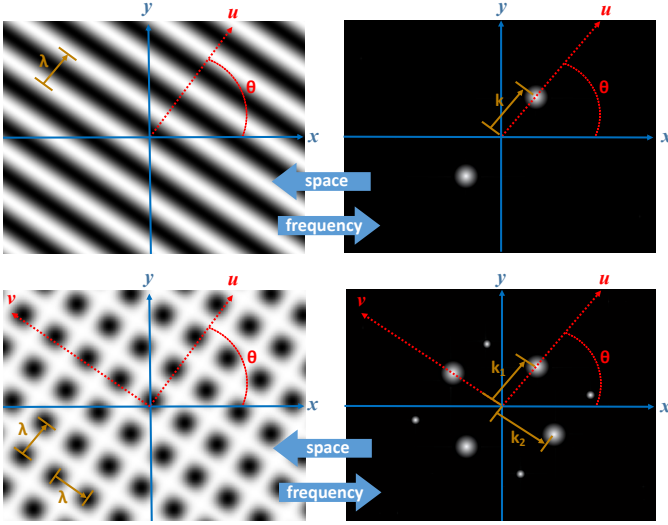
Fig. 1. Illustration of the link between spatial and frequency domains in the simple cases of 2-D spatial sinusoid directed along one then two directions.

where θ is the angle of the pattern, $a_{n,m,\theta}$ the analysis function given by:

$$a_{n,m,\theta} = e^{-2\pi i \left(\frac{k_1 n}{N} + \frac{k_2 m}{M}\right)} \qquad (11)$$

with $\frac{k_1}{N} = \frac{\cos(\theta)}{\lambda}$, $\frac{k_2}{M} = \frac{\sin(\theta)}{\lambda}$ and $h_{n,m}$ a 2-D Gaussian window given by:

$$h_{n,m} = e^{-\left(\frac{n-N/2}{\sigma_1}\right)^2 - \left(\frac{m-M/2}{\sigma_2}\right)^2} \qquad (12)$$

In this way, displacements along the axis $\mathbf{u}$ and $\mathbf{v}$ (see Fig. 1) of the pattern are obtained, similarly to the 1D case (5), with:

$$\begin{cases} \hat{d}_u = \frac{\hat{\phi}_{0,0,\theta} \cdot \lambda}{2\pi} + p\,\lambda \\ \hat{d}_v = \frac{\hat{\phi}_{0,0,\theta+\frac{\pi}{2}} \cdot \lambda}{2\pi} + q\,\lambda \end{cases} \qquad (13)$$

The last step is to transfer these results into the basis $(\mathbf{x}, \mathbf{y})$ of the image:

$$\begin{cases} \hat{d}_x = \hat{d}_u \, \cos(\theta) - \hat{d}_v \, \sin(\theta) \\ \hat{d}_y = \hat{d}_u \, \sin(\theta) + \hat{d}_v \, \cos(\theta) \end{cases} \qquad (14)$$

B. 2-D Frequency and Angle Tracking

The angle of the pattern and its period can be determined in the frequency domain (see Fig. 1). Here, we begin by the measurement of the angle:

$$\hat{\theta} = \arctan 2\left(\frac{\partial \varphi}{\partial y}, \frac{\partial \varphi}{\partial x}\right) \qquad (15)$$

Using the CFD principle and the previous notations give:

$$\theta = \arctan 2(\Delta_y, \Delta_x) \qquad (16)$$

with the two differences defined with 4 complex obtained with (10): $\Delta_x = \phi_{x+1,y} - \phi_{x-1,y}$ and $\Delta_y = \phi_{x,y+1} - \phi_{x,y-1}$.
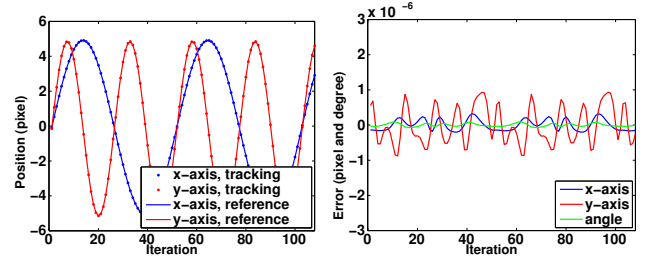

Fig. 2. Position of the pattern (left) and error with the reference (right) obtained by simulation during a displacement in translation of the pattern. The error is lower than 10^{-6} pixel in translation and 10^{-7} rad in rotation.

Then, we calculate the period of the pattern along the axis $\mathbf{u}$. As in 1D measurement, the frequency can be computed with the phase change for continuous signal by:

$$f = \frac{1}{2\pi} \frac{d\varphi}{du} = \frac{1}{2\pi} \left(\frac{\partial \varphi}{\partial x} \frac{\partial x}{\partial u} + \frac{\partial \varphi}{\partial y} \frac{\partial y}{\partial u}\right) \qquad (17)$$

Therefore, using the CFD in $\mathbf{x}$ and $\mathbf{y}$ directions we get:

$$\hat{k} = \frac{1}{4\pi}\left(\Delta_x \cos(\theta) + \Delta_y \sin(\theta)\right) \qquad (18)$$

Finally, we know that $\theta = \arctan 2(\Delta_y, \Delta_x)$. So it is possible to remove θ from equation (18):

$$\hat{k} = \frac{1}{4\pi}\sqrt{\Delta_x^2 + \Delta_y^2} \qquad (19)$$

The same method allows computing the period along the v axis.

C. Simulation Validation Tracking

The performances of the measure were tested in simulation with MatLab. From an initial pose with an angle of 22.5 degrees, a perfect sinusoidal pattern (period of 15 pixels) was displaced in translation (Fig. 2). During this simulation, the periods were permanently computed with an error lower than 10^{-7} pixel. The others errors are illustrated in Fig. 2. Moreover, the calculations were made in less than 0.05 second by iteration, completely compatible with a real-time application.

The variation of the other parameters (angle, period) gives similar performances, notably with an error of 10^{-4} pixel for the period estimation and of $2 \cdot 10^{-7}$ rad for the angular position estimation.

IV. 3-DoF VISUAL SERVOING

The tracking algorithm computes the pose of the image pattern. Since the period of the actual pattern is known, the displacements are directly given in a metric way without any need for camera or robot calibration.

Let $\mathcal{R}_I$ and $\mathcal{R}_P$ be the frames attached to the image and to the pattern, respectively. The tracking algorithm provides, for each new image, the homogeneous transformation between $\mathcal{R}_I$ and $\mathcal{R}_P$ such as:

$$^I\mathbf{M}_P = \begin{bmatrix} ^I\mathbf{R}_P & ^I\mathbf{t}_P \\ \mathbf{0} & 1 \end{bmatrix} \qquad (20)$$

with $^I\mathbf{R}_P$ the $3{\times}3$ rotation matrix and $^I\mathbf{t}_P$ the $3{\times}1$ translation vector.

The control law aims to move the pattern to a given position defined by the frame $\mathcal{R}_{I^*}$. To get a straight line trajectory in the image, we choose a regular scheme proposed in [21]. This scheme consists of choosing $\mathbf{s} = (^I\mathbf{t}_P, \theta\mathbf{u})$ as the current 3D pose and $\mathbf{s}^* = (^{I^*}\mathbf{t}_P, \mathbf{0})$ as the pose of the pattern relative to the desired image frame $\mathcal{R}_{I^*}$. The notation $\theta\mathbf{u}$ is the angle/axis parameterization of the rotation. In this case, the error is:

$$\mathbf{e} = (^I\mathbf{t}_P - {}^{I^*}\mathbf{t}_P, \theta\mathbf{u}) \quad (21)$$

and the interaction matrix related to $\mathbf{e}$ is defined by,

$$\mathbf{L}_e = \begin{bmatrix} -\mathbf{I}_3 & \left[^I\mathbf{t}_P\right]_\times \\ \mathbf{0} & \mathbf{L}_{\theta\mathbf{u}} \end{bmatrix} \quad (22)$$

where $\mathbf{I}_3$ is the $3{\times}3$ identity matrix, $\left[^I\mathbf{t}_P\right]_\times$ the skew matrix of $^I\mathbf{t}_P$ and $\mathbf{L}_{\theta\mathbf{u}}$ is the interaction matrix defined in [22].

The control law gives the robot spatial velocities $\mathbf{v} = (\mathbf{v}_x, \mathbf{v}_y, 0)$ and $\boldsymbol{\omega} = (0, 0, \boldsymbol{\omega}_z)$ as:

$$\begin{bmatrix} \mathbf{v} \\ \boldsymbol{\omega} \end{bmatrix}_{\mathcal{R}_I} = -\gamma \mathbf{L}_e^+ \mathbf{e} \quad (23)$$

with $\mathbf{L}_e^+$ a pseudo-inverse of the interaction matrix defined by:

$$\mathbf{L}_e^+ = \begin{bmatrix} -\mathbf{I}_3 & \left[^I\mathbf{t}_P\right]_\times \mathbf{L}_{\theta\mathbf{u}}^{-1} \\ \mathbf{0} & \mathbf{L}_{\theta\mathbf{u}}^{-1} \end{bmatrix} \quad (24)$$

After developments, the control law can be written as,

$$\begin{bmatrix} \mathbf{v} \\ \boldsymbol{\omega} \end{bmatrix}_{\mathcal{R}_I} = \begin{bmatrix} -\gamma((^{I^*}\mathbf{t}_P - {}^I\mathbf{t}_P) + \left[^I\mathbf{t}_P\right]_\times \theta\mathbf{u}) \\ -\gamma\theta\mathbf{u} \end{bmatrix} \quad (25)$$

Considering our task, since only the x, y and θ DoF are taken into account. Thus, we obtain the coupled control:

$$\begin{cases} \mathbf{v}_x &= -\gamma((x^* - x) + y\theta) \\ \mathbf{v}_y &= -\gamma((y^* - y) - x\theta) \\ \boldsymbol{\omega}_z &= -\gamma\theta \end{cases} \quad (26)$$

V. EXPERIMENTAL RESULTS

The developed materials were confronted to evaluating tests in order to demonstrate its performances in terms of convergence rate, accuracy and robustness (still working under external disturbances).

A. Experimental Setup

The method was tested on an eye-to-hand experimental setup (Fig. 3) composed by a Fireware CCD monochrome camera (Allied Vision Technology Guppy F-046, $640{\times}480$ pixels) used at 3.75 frames per second (fps) with a macro-objective directed towards the planar target (a periodic pattern). The latter is fixed on a microrobotic platform including a rotation actuator (SR-3610-S from SmarAct; range $= 2\pi$; resolution $= 0.17$ µrad) and two translation actuators (M-111-1DG from Physic Instrumente; range $= 15$ mm; unidirectional repeatability $= 0.1$ µm; backslash =
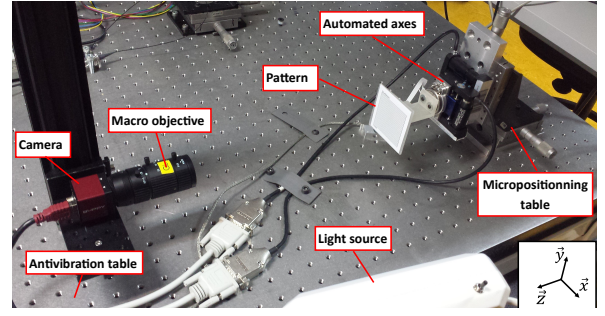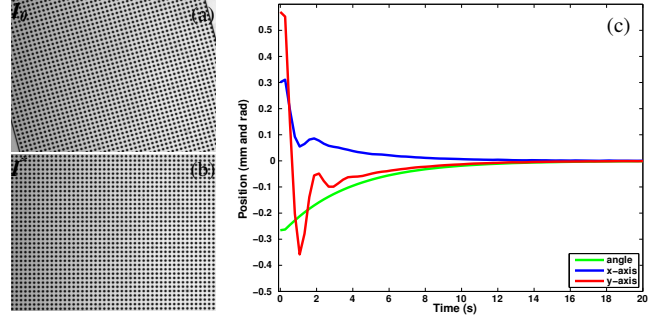

Fig. 3. Experimental setup of visual servoing.

Fig. 4. Experimental validation under nominal conditions. (a) Initial image; (b) desired image; (c) the error decay in each DoF versus time. Final error below 1 µm and 0.02 mrad.

2 µm). The setup is mounted on an antivibration table and illuminated with a controlled light source. The controller was implemented with MatLab on a PC: Intel Core2 Quad CPU Q9550 2.83 GHz running under Windows 7.

The pattern used is composed of points with a 1 mm periodicity along $\mathbf{x}$ and $\mathbf{y}$ axes, distributed in a $50{\times}50$ mm square.

B. Validation on Favorable Conditions

The method was firstly tested in nominal conditions of use (stable lightning source, without occlusions, etc.). Again, it can be highlighted that the controller works without any calibration step. The pattern was arbitrarily positioned along $\mathbf{x}$ and $\mathbf{y}$ axes, and the initial angle θ_0 is 15 degrees (Fig. 4.a). The control loop (image acquisition, Fourier Transform, etc.) runs at a frequency of 2 Hz.

Only 30 iterations are sufficient to reach the desired positions (see Fig. 4). The obtained accuracy when the controller reaches the desired position is estimated (using the robotic encoders) to 1 µm.

C. Unfavorable Conditions

Additional experimental tests were performed in order to demonstrate the robustness of our method under different external disturbances.

The first experiment is about focus. In this test, it will be shown that the controller can perfectly work under blurred images. As can be seen on Fig. 5, the frequency measurement
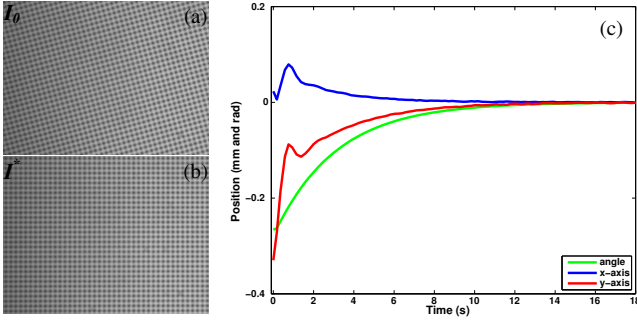
Fig. 5. Experimental validation using blurred images. (a) Initial image; (b) desired image; (c) the error decay in each DoF versus time. Final error below 2 μm and 0.05 mrad.
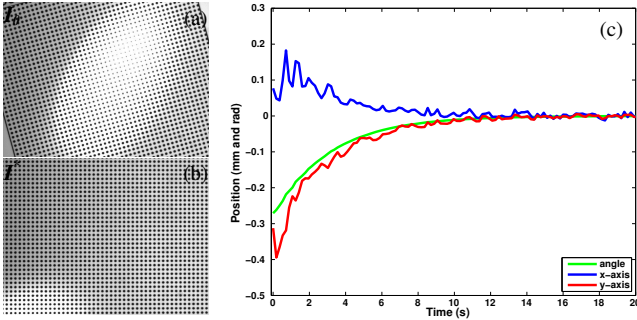

Fig. 6. Experimental validation under unstable lightning. (a) Initial image; (b) desired image; (c) the error decay in each DoF versus time. Final error below 10 μm and 0.1 mrad.
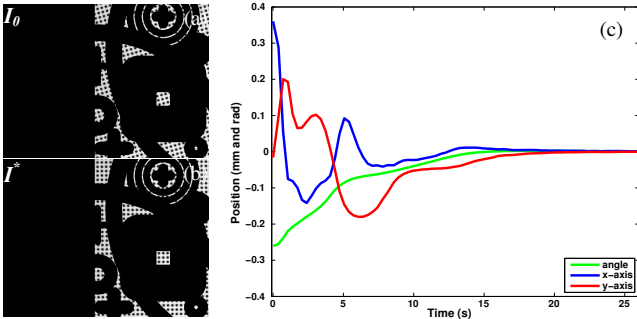

Fig. 7. Experimental validation under partial occlusions. (a) Initial image; (b) desired image; (c) the error decay in each DoF versus time. Final error below 2 μm and 0.1 mrad.
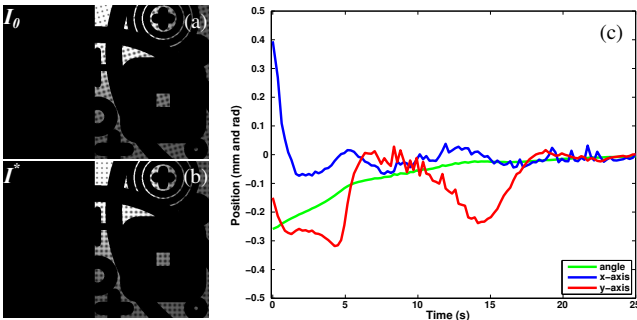

Fig. 8. Experimental validation using blurred images, partial occlusion and specularity. (a) Initial image; (b) desired image; (c) the error decay in each DoF versus time. Final error below 30 μm and 1 mrad.
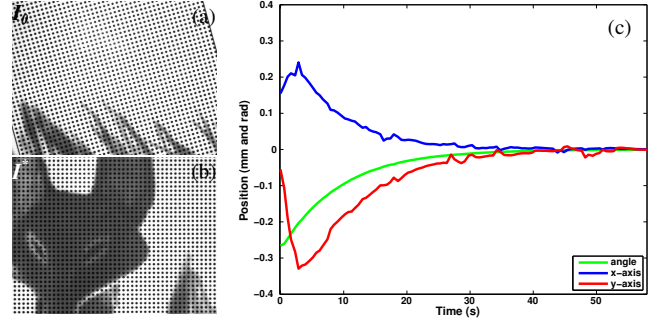

Fig. 9. Experimental validation using a variable source of noises. (a) Initial image; (b) desired image; (c) the error decay in each DoF versus time. Final error below 10 μm and 0.2 mrad.

remains efficient and thus the controller converges easily to the desired position.

To test the effect of the specularity on our method, the pattern was enlightened with a concentrated light source. Tests were made by displacing arbitrarily the light on the pattern (see Fig. 6). The experiments always lead to convergence, but the light affect the period estimation and consequently the translation error which is noised (accuracy of 10 μm).

To observe the impact of occlusion on our method, we generate arbitrary black shapes on our image. These shapes are constant during the servoing. We applied an occultation area up to 90 % of the image. Fig. 7 shows that the major effect is a less direct convergence. However the final accuracy is not affected.

To go even further in the analysis of the robustness of the method, we tested it with, in the same time, the three perturbations previously exposed (blur, light variation and occlusion). Fig. 8 shows that the method always converges. However it combines the defaults observed in the previous tests (indirect convergence and noise on the translating axes).

We concluded on the robustness of the method with a noise experiment: we projected a movie on the pattern during the visual servoing (*The Little Prince* by Mark Osborne). As exposed in Fig. 9, the convergence is made with a micrometric final accuracy.

D. Depth Measurement

Finally, an additional validation test was performed considered as an extension of the controller to 4 DoF visual servoing. The idea is to use the period measurement to measure the depth of the pattern (its position along the z-axis). Indeed, a displacement d_z in the camera's axis introduces a proportional period variation from λ_0 to λ_z:

$$d_z = c_0\left(\frac{\lambda_z}{\lambda_0} - 1\right) \qquad (27)$$

However, such a measure requires a calibration step to determine the coefficient c_0 linked to λ_0. But, in a context allowing this calibration step, a visual servoing can be made with similar performances to those realized previously. Indeed, by moving the pattern with the manual micropositionning table (in nominal conditions), we obtain measurements made along
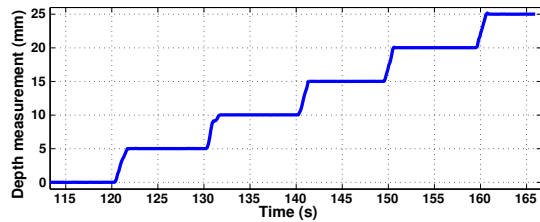
Fig. 10. Depth estimating using the period measurement of the pattern. The pattern was moved manually with a micropropositioning table. A preliminary calibration step is required to realize this measure. The error is below 20 μm.

the z-axis on a 25 mm range with an accuracy better than 10 μm without setting the focus (see Fig. 10).

VI. CONCLUSION

In this paper, it was presented a new 3 DoF (2 translations, 1 rotation) visual servoing method based on the single phase measurement of a periodic pattern. The main advantages of the proposed method are accuracy, robustness and does not require any calibration step.

This method was validated experimentally on micro-robotic platform in both favorable conditions (stable light-ning source, small displacements) as well as unfavorables ones (blurred images, lightning changes, partial occlusion, or combining several above disturbances). The obtained results demonstrated the efficiency of the controller, this in different terms of performances. For instance, the obtained accuracy (1 μm on translation axes and 10^{-4} rad on rotation axis) and convergence rate (30 iterations in favorable conditions). Also the control law shows an interesting robustness with respect to lightning changes, partial occlusion (90 % of the image), etc. Additionally, a measure along a fourth degree of freedom (the depth) was realized with as prerequisite an additional calibration step.

The demonstrated performances of this controller allows to consider others applications, for instance it may be concern especially the nanorobotic applications when accuracy and robustness are the main objectives. Also, nanoforce mea-surements and mechanical characterizations, especially for medical purposes (in-vivo oocyte properties study).

REFERENCES

[1] D. Popa, R. Murthy, and A. Das, "M3-deterministic, multiscale, multirobot platform for microsystems packaging: Design and quasi-static precision evaluation," *IEEE Transaction on Automation Science and Engineering*, vol. 6, no. 2, pp. 345–361, 2009.

[2] E. Lubrano, M. Bouri, and R. Clavel, "Ultra-high-precision industrial robots calibration," in *IEEE International Conference on Robotics and Automation*, Shanghai, 2011, pp. 228–233.

[3] N. Tan, C. Clevy, G. J. Laurent, P. Sandoz, and N. Chaillet, "Accuracy quantification and improvement of serial micropositioning robots for in-Plane motions," *IEEE Transaction on Robotics*, vol. 31, no. 6, pp. 1497–1507, 2015.

[4] N. Tan, C. Clévy, and N. Chaillet, "Calibration of single-axis nanopo-sitioning cell subjected to thermal disturbance," in *IEEE International Conference on Robotics and Automation*, Karlsruhe, Germany, 2013, pp. 3645–3650.

[5] B. Espiau, F. Chaumette, and P. Rives, "A new approach to visual servoing in robotics," *IEEE Transactions on Robotics and Automation*, vol. 8, no. 3, pp. 313–326, 1992.

[6] E. Marchand and C. Collewet, "Using image gradient as a visual feature for visual servoing," in *IEEE/RSJ International Conference on Intelligent Robots and Systems*, 2010, pp. 5687–5692.

[7] B. Tamadazte, G. Duceux, N. Le-Fort Piat, and E. Marchand, "Highly precise micropositioning task using a direct visual servoing scheme," in *IEEE International Conference on Intelligent Robots and Systems*, 2011, pp. 5689–5694.

[8] E. Marchand, F. Chaumette, F. Spindler, and M. Perrier, "Mutual information-based visual servoing," *IEEE Transactions on Robotics*, vol. 27, no. 5, pp. 958–969, 2011.

[9] N. P. Papanikolopoulos and P. K. Khosla, "Adaptive robotic visual tracking: Theory and experiments," *IEEE Transaction on Automatic Control*, vol. 38, no. 3, pp. 429–445, 1993.

[10] W. Huang, C. Ma, and Y. Chen, "Displacement measurement with nanoscale resolution using a coded micro-mark and digital image correlation," *Optical Engineering*, vol. 53, no. 12, pp. 124 103–1:7, 2014.

[11] M. Ourak, B. Tamadazte, and N. Andreff, "Wavelets-based 6 DOF visual servoing," in *IEEE International Conference on Robotics and Automation (accepted for publication)*, 2016.

[12] L.-A. Duflot, A. Krupa, B. Tamadazte, and N. Andreff, "Towards ultrasound-based visual servoing using shearlet coefficients," in *IEEE International Conference on Robotics and Automation (accepted for publication)*, 2016.

[13] J. Gao, C. Picciotto, W. Wu, and W. Tong, "From nanoscale dis-placement sensing and estimation to nanoscale alignment," *Journal of Vacuum Science & Technology B: Microelectronics and Nanometer Structures*, vol. 24, p. 3094, 2006.

[14] C. Yamahata, E. Sarajlic, G. Krijnen, and M. Gijs, "Subnanometer translation of microelectromechanical systems measured by discrete fourier analysis of ccd images," *Microelectromechanical Systems, Journal of*, vol. 19, no. 5, pp. 1273–1275, 2010.

[15] D. Boyton, "Position encoder using statistically biased pseudorandom sequence," 2003, uS Patent App. 10/399, 470.

[16] J. Galeano Zea, P. Sandoz, E. Gaiffe, S. Launay, L. Robert, M. Jacquot, F. Hirchaud, J.-L. Prétet, and C. Mougin, "Position-referenced mi-croscopy for live cell culture monitoring," *Biomedical optics express*, vol. 2, no. 5, pp. 1307–1318, 2011.

[17] J. Galeano-Zea, P. Sandoz, E. Gaiffe, J. Prétet, and C. Mougin, "Pseudo-periodic encryption of extended 2-D surfaces for high ac-curate recovery of any random zone by vision," *International Journal of Optomechatronics*, vol. 4, no. 1, pp. 65–82, 2010.

[18] V. Guelpa, G. J. Laurent, P. Sandoz, and C. Clévy, "Vision-based microforce measurement with a large range-to-resolution ratio using a twin-scale pattern," *IEEE/ASME Transaction on Mechatronics*, vol. 20, no. 6, pp. 3148–3156, 2015.

[19] A. Ferreira and R. Sousa, "DFT-based frequency estimation under har-monic interference," in *International Symposium on Communications, Control and Signal Processing*, 2010, pp. 1–6.

[20] B. Boashash, "Estimating and interpreting the instantaneous frequency of a signal. II. Algorithms and Applications," in *Proceedings of the IEEE*, vol. 80, no. 4, 1992, pp. 520–538.

[21] E. Marchand, F. Chaumette, F. Spindler, and M. Perrier, "Controlling an uninstrumented manipulator by visual servoing," *The International Journal of Robotics Research*, vol. 21, no. 7, pp. 635–647, 2002.

[22] E. Malis, F. Chaumette, and S. Boudet, "2 1/2D visual servoing," *IEEE Transactions on Robotics and Automation*, vol. 15, no. 2, pp. 238–250, 1999.